Molecular Systems Design & Engineering

REVIEW

View Article Online
View Journal | View Issue

Cite this: *Mol. Syst. Des. Eng.*, 2016, **1**, 370

A road towards 25% efficiency and beyond: perovskite tandem solar cells

T. Todorov,*[a] O. Gunawan[a] and S. Guha[b]

Received 3rd May 2016,
Accepted 20th July 2016

DOI: 10.1039/c6me00041j

rsc.li/molecular-engineering

For decades, the appealing potential of tandem solar cells for efficiencies beyond the single-junction Shockley–Queisser limit has led researchers to develop thin film tandem solutions for high performance low cost solar cells. Perovskite solar cells have recently emerged as a promising candidate for photovoltaics. In addition to ease of fabrication and good efficiencies, a particularly attractive feature is their tunable band gap between 1.48 and 2.3 eV that enables symbiosis with other solar cells in tandem device configurations. The low-temperature processing conditions of perovskites make it possible to monolithically integrate them as the top component of tandem structures without damaging the bottom cell. Early experimental results and modelling indicate that efficiencies beyond 25% are within reach. Optimization and solving perovskite stability limitations could result in a commercially viable technology. We review recent developments and insights in the field.

Design, System, Application

We review the most relevant design strategies of tandem solar cells for enhanced solar spectrum harvesting. For practical applications, monolithic tandem solar cells offer significant advantages over 4-terminal devices typically used for lab demonstrations. However, achieving functional monolithic tandems on polycrystalline solar cells has been a difficult task until recently due to junction degradation during high-temperature processing. At the same time, achieving a high-efficiency, high-band gap partner for polycrystalline bottom absorbers has also been challenging. Another challenge for the design and optimization of functional low-cost two-terminal devices for photovoltaic applications is the difficult characterization of the individual cells, especially in cases where degradation may occur when one is fabricated on top of the other. Perovskite solar cells offer for the first time the unique combination of high efficiency at high (and tunable) band gap, coupled with relatively low processing temperature that does not impair the functionality of the bottom absorber. This dramatically extends the range of design possibilities as evidenced by multiple demonstrations of high-efficiency monolithic tandem solar cell structures including *in situ* band gap engineered perovskite absorbers on top of chalcogenide bottom cells. Resolving the stability challenges of perovskites would make them an ideal partner in two-terminal tandem devices for solar energy conversion applications.

A. Introduction

The modern single p–n junction based solar cell, first proposed in the 1950s,[1] has come a long way so that photovoltaic technologies are beginning to be economically viable today.[2] Progress has occurred over decades, using silicon and other material technologies, often resulting in long progress plateaus with an uncertain path for further growth, and funding cycles that have been influenced by the price of fossil fuels. Commercial single p–n junction devices vary in efficiencies today between around 12% and 24%, at different cost to performance ratios and for different materials that are either crystalline, large/single grained substrate based (such as silicon and GaAs) or polycrystalline films grown on glass (such as CuInGaSe and CdTe).[3] Regardless of the state of development, no single junction technology can realistically overcome the Shockley–Queisser limit of about 33%.[4] The use of multi-junction solar cells, where two or more absorbing photovoltaic cells are monolithically connected on top of one another, allows higher efficiencies to be reached. However, multi-junction or tandem (when the number of junctions equals two) solar cells have found only a limited range of product applications due to issues with either cost, inadequate efficiency or material and process compatibility.

Of all available solar cell combinations, only two technologies have been able to develop monolithically integrated two-terminal tandem devices (described below as type A) that could reach the market. The first is amorphous silicon based, and is an example of a relatively low-cost and low efficiency solar cell that is still a viable solution for consumer electronic products (*e.g.* electronic calculators).[5] On the other end of the performance (and cost) scale are the III–V multi-junction solar cells that hold the current efficiency record (46% using GaInP/GaAs; GaInAsP/GaInAs (ref. 6)), were the first to

[a] *IBM T. J. Watson Research Center, P. O. Box 218, Yorktown Heights, NY, 10598, USA. E-mail: tktodoro@us.ibm.com*
[b] *Center for Nanoscale Materials (CNM), Argonne National Laboratories, Argonne IL 60439, USA; Institute for Molecular Engineering, University of Chicago, Chicago IL 60615, USA*

surpass the Shockley–Queisser limit and are currently the standard solution for highest efficiency concentrator and PV applications in space. Multi-junction or tandem solar cells using other major photovoltaic materials such as crystalline silicon, CdTe and CIGS have met significant fabrication challenges for monolithic integration and have been used mostly in multi-terminal lab tandem demonstrations (described below as type B). The new perovskite materials have emerged as a possible solution, provided that design optimization and serious issues with stability and environmental friendliness can be resolved.

B. Tandem device classifications

Multi-junction solar cells and their advantages for efficiently absorbing a wider range of the solar spectrum have been described in detail elsewhere.[7] For optimal absorption, p–n junctions with a higher band-gap are stacked on top of those with a lower bandgap. In this fashion, higher energy photons from the incident solar radiation are more efficiently absorbed by the high band gap layers at the top, thereby minimizing the difference between the photon energy and the absorber band gap energy, *i.e.* the energy unavailable for electrical energy conversion. The multiple p–n junctions are electrically connected *via* tunnel junctions or a shared electrode, resulting in a series electrical connection.

In this review, we limit ourselves to two-junction tandem devices that operate under planar, non-concentrated light (*i.e.* 1 sun AM1.5G illumination). There are several types of tandem solar cells depending on the fabrication sequence and interconnection scheme used. In this work, we classify them as type A and B based on the number of transparent conductive electrodes (TCEs) and the number of their contact terminals that ranges from two to four. We will use this abbreviation instead of the common TCO (transparent conductive oxide) because there are cases where the standard in industry doped conductive oxides such as ZnO : Al, In_2O_3 : Sn and SnO_2 : F is difficult to adapt for some tandem applications due to temperature and/or sputtering damage on the underlying structures even with protective inter-layers. Alternative examples include transparent conductive layers of graphene, carbon nanotubes, and silver nanowires or thin metal films.[8–11]

Type A tandem is a monolithic series interconnected device grown on a single substrate that employs one TCE (Fig. 1a), which implies that it is a two-terminal (2-T) tandem device. This is the configuration almost exclusively used in commercial products because it involves a minimum number of processing steps, substrates, layers and interconnections. Because these are essentially two back to front solar cells monolithically stacked on top of one another, the performance of the tandem relies on the efficiency of the charge transport layer at the interface between the two solar cell components. Type B tandem solar cells (Fig. 1b–d) bypass this challenge by using additional transparent conductive layers and substrates; this type includes a 2-T (two terminal) mechanically stacked device, 3-T, and 4-T tandems. This way the individual devices from the stack can be fabricated independently, thereby also significantly expanding the processing tolerance window as well as simplifying the full device characterization.

While the type B tandem is convenient for research and feasibility demonstration purposes, it is impractical for large scale manufacturing. The single transparent TCE layer is one of the most critical components for large-scale applications from both a manufacturing and a performance perspective. Firstly, the TCE is a key contributor to the manufacturing cost of the photovoltaic module since it requires expensive and low throughput sputtering or CVD equipment. Secondly, the design of the TCE is always an inherent trade-off between optical and series resistance losses that typically reduce the overall module efficiency by 10–25%.[12] Additionally, a single TCE allows monolithic module integration of multiple tandem stacks on a large-area substrate with simple scribing procedures, which is much more cost-efficient than external wiring. It is therefore difficult to imagine a competitive large-scale module production employing a B-type solar cell with more than one TCE.[13] However, research and development of type A solar cells is extremely challenging because it requires compatibility of every processing step with all preceding

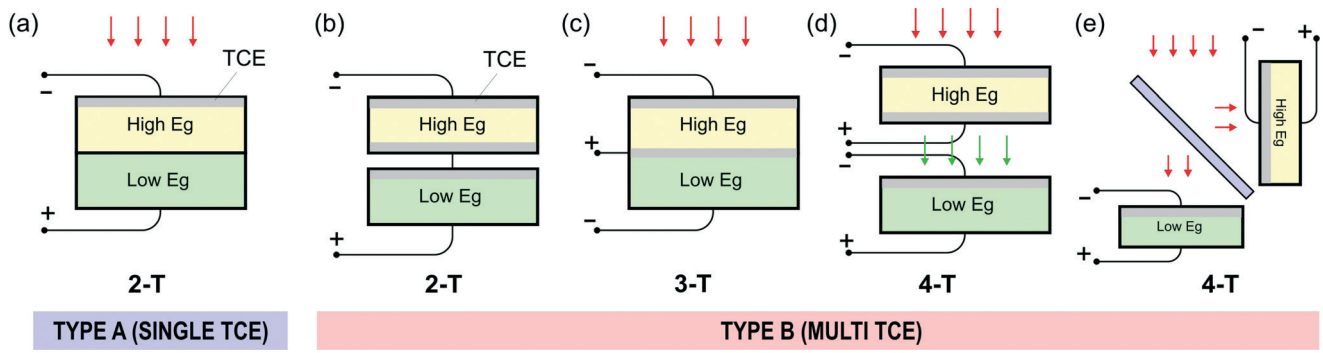

Fig. 1 Types of tandem solar cell device based on the number of TCEs and terminal connections: (a) type A: single TCE, two-terminal monolithic; and type B with multiple TCEs: (b) two-terminal mechanically stacked, (d) 4-terminal mechanically stacked, (c) 3-terminal monolithic stack and (e) 4-terminal spectrum-split.

layers and interfaces as well as precise optical and current matching between individual devices. Characterization of the type A structure is also challenging because device isolation in the stack is difficult or even impossible without auxiliary elements such as intermediate TCO.

Naturally, type B is the configuration of choice for most research focused on non-traditional tandem solar cell concepts. A comparison of experimental and theoretical properties of devices or the different types is presented below.

We elaborate the characteristics of each type of tandem devices as follow:

(1) Type A/two-terminal monolithic stack

As described in the introduction, this tandem device is constructed from a monolithically integrated bottom and top cell with a single transparent conductive layer. A recombination or tunneling layer is formed between the two devices. The main electrical limitation in these devices is the current matching condition *i.e.* the performance of the device is limited by the cell with the lowest current. However, this architecture is attractive in terms of simplicity for commercial deployment as only two terminals are required and a monolithic series interconnection of narrow device architectures on a single substrate is feasible with the standard scribing technology thus reducing the series resistance losses associated with large-area modules.

(2) Type B/two-terminal mechanically-stacked

The tandem device is constructed as a stack of two separate top and bottom cells but they are serially connected with two terminal output. This type of tandem has the advantage where the need for interfacial tunneling is eliminated and the current matching condition can be relaxed by adjusting different areas of the solar cell. However, these devices require as many as three TCE layers and thus impose severe optical losses.

(3) Type B/three-terminal monolithic stack

Similar to the two-terminal tandem, the device is constructed from a monolithically integrated bottom and top cell – however, a third intermediate terminal is provided. This terminal adds another degree of freedom in the electrical connection to relieve the circuit from the current matching condition. This can be done by adding a matching resistive load to either the top or bottom cell. This type of device is not frequently explored (for the reason explained in the next section) but nevertheless they have been demonstrated in a tandem a-Si solar cell,[14] GaAsP/SiGe device[15] and polymer solar cell.[16] There has been no demonstration of the 3-T tandem using perovskite cells so far.

(4) Type B/four-terminal mechanically stacked

The tandem device is constructed from two separately developed cells that allow a fabrication process that yields optimum performance. However, bifacial transparent electrodes are needed on the top cell to allow some light transmission to the bottom cell. Each cell produces independent electrical output thus requiring 4 terminal connections. While efficiency can be maximized, the interconnection and module integration could become more costly. A recent example of this type of perovskite tandem device has reached an efficiency of 25.2% and[17] 18.6% with perovskite–silicon and perovskite–CIGS tandem, respectively.[11]

(5) Type B/four-terminal spectrum split

This architecture is essentially still a four terminal device, however a dichroic filter is used to split the light spectrum. This system offers advantages in terms of flexibility of individual device fabrication *i.e.* each device can be optimized as if it operates as a stand-alone solar cell and only requires two TCEs (instead of three as in the standard 4-T tandem) – thus reducing the optical loss. However, the added cost of filter and four terminals limits the commercial potential of this architecture. An example of this type of tandem has been demonstrated by Uzu *et al.* with an impressive total potential efficiency of 28.0%.[18]

C. Theoretical limit of the idealized tandem cells

We discuss the general device characteristics and bandgap optimization issue of two-junction tandem devices. To obtain a general understanding of tandem cell performance with regard to various terminal configurations, it is sufficient to consider a simple idealized, Schottky–Queisser (SQ) limit-like tandem cell calculation.[19] We use unconcentrated 1 sun AM1.5G solar spectrum as the input illumination in the calculation. In a SQ single junction model, only photons with energy above the bandgap can be absorbed and contribute to photocurrent. The hot charge carrier generated by these photons will relax down to the bandgap energy in the process called "thermalization". Considering radiative and non-radiative recombination of the carriers, we obtain 33.7% limit for a single junction solar cell at a bandgap of 1.34 eV.[20]

In our SQ-like tandem calculation, we use a fixed silicon bottom cell (E_{g1} = 1.1 eV) with a SQ-limit efficiency of 32.9%. The top cell has a higher and varying bandgap E_{g2} which serves as an independent variable. The top cell also operates at the SQ limit. We assume no optical loss (other than the absorption due to the top cell's absorber) so that all photons below E_{g2} are transmitted to the bottom cell: in other words, the bottom cell is filtered (shadowed) by the top cell. In reality, there are reflective losses due to various interfaces in the top cell that also reduce the photons below E_{g2}. On the other hand, there is some quantum efficiency response for the bottom cell for photons above E_{g2} due to incomplete absorption of the top cell. These two effects work in opposite directions and they tend to reduce and increase the J_{sc} of the bottom cell, respectively. The J–V curves of the bottom Si cell

(filtered) and the top cell with bandgap E_{g2} = 2.0 eV are shown in Fig. 2(a). The details of the SQ limit calculation are given in ref. 19 and 20.

For comparative evaluation, we calculate the performance of each type of tandem configuration as follows:

(1) Four-terminal (4-T) tandem

Each of the cells operates independently and the tandem efficiency is simply the sum of each individual cells. Fig. 2(b) shows the 4-T tandem efficiency (green curve) as a function of top cell bandgap; it is clear that the 4-T configuration yields the best total efficiency (Eff ~ 45%[21]) compared to other tandem configurations (at the expense of more complicated wiring as discussed earlier).

(2) Three-terminal (3-T) tandem

The cells essentially operate in parallel with one common terminal (either anode or cathode). The top and bottom terminals are also joined outside the cell to complete the parallel connection. In this tandem, the voltage is limited by the lowest voltage and the total current is the sum of each individual current. In Fig. 2(b), the efficiency of this type of tandem is practically flat, independent of the top cell bandgap. The reason is that the V_{oc} is fixed as it is limited by the bottom cell (1.1 eV) and the total current density is also practically fixed as both the top and bottom cells are assumed to have 100% single-junction efficiency. This results in a constant efficiency profile yet it is always worse than the 4-T tandem.

(3) Two-terminal (2-T) tandem

The cells are connected either monolithically or by mechanical stacking. In this tandem, the current is limited by the cell with lower current and the voltage is added in series. As a result, the efficiency profile strongly varies with respect to the top bandgap (E_{g2}) with a peak performance at E_{g2} = 1.72 eV. Note that at this optimum bandgap, the 2-T tandem practically performs the same as the 4-T tandem as both cells achieve the same current density (thus no power loss due to current matching condition). This optimum bandgap value is also close to the value of 1.8 eV from the more elaborate Si–perovskite 2-T tandem cell modeling in ref. 11.

From the efficiency comparison chart in Fig. 2, we can draw several conclusions that apply to the tandem cell development in general. First, the 2-T tandem cell will perform the same as the 4-T tandem at its optimum bandgap, while offering the benefits of cheaper and more scalable manufacturing. Second, the maximum efficiency of the 2-T tandem (red dot) is also close to that of the 4-T tandem (green dot). Third, the maximum efficiency of the 3-T tandem is lower compared to those of the 2-T and 4-T tandems – thus it is reasonable that this type of tandem cell is not widely pursued.

D. Progress and challenges for perovskite tandem cells

Until recently, apart from thin film silicon and III–V materials, attempts to develop tandem solar cells have had limited success. The two main challenges for type A solar cells have been: (1) achieving efficient high-band gap top cells (especially for chalcogenide photovoltaics) and (2) processing incompatibilities such as junction deterioration due to high-temperature processes or other processes such as sputtering damage. These limitations are particularly critical for high-efficiency chalcogenide photovoltaics where – in addition to increased V_{oc} deficit at high band gaps,[22,23] – severe junction deterioration is observed at temperatures exceeding 200 °C. As a result, before the introduction of organic and perovskite cells, most examples of tandem devices included 4-terminal stacked configurations such as CIGS–CdTe,[24] CIGS-dye sensitized solar cells,[25] CIGS–CGS[26] and CIGS–CIGS[27] cells with different ratios of In : Ga. With the development of organic solar cells that allow low processing temperatures, research on monolithic type A tandems has increased. Organic layer transfer on CIGS yielded 3.7% efficiency.[28] Multiple examples of all-organic polymer tandem solar cells have also been reported reaching efficiencies up to 11%.[29–31]

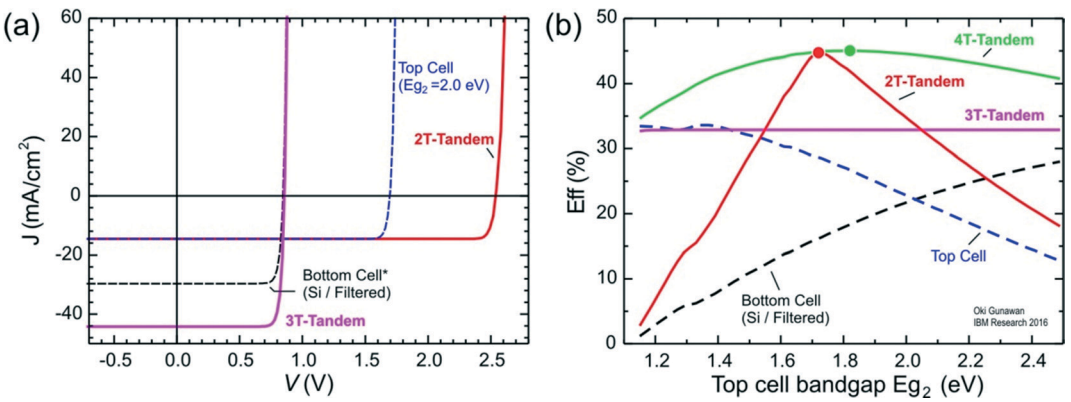

Fig. 2 Performance comparison of various tandem configurations (2, 3 and 4 terminals) based on idealized SQ-limit calculation *vs.* bandgap of the top cell. The bottom cell is Si (1.1 eV) which is filtered by the top cell: (a) *J*–*V* curves under AM1.5G 1 sun light for the top cell with E_{g2} = 2.0 eV. (b) Efficiencies of the constituent cells and the tandem cells.

We present the current status of various perovskite tandem devices that have been reported in the literature in Table 1. The advent of perovskite photovoltaics with the fastest efficiency progress in history currently reaching over 20%[39,40] with band gaps above 1.5 eV brought multiple new opportunities for monolithic tandem solar cells. The possibility of depositing them in either p–n or n–p sequence and the easily tunable band gap within the 1.48–2.3 eV range[17] make them ideal for engineering optical and current matching.[37] The low processing temperature allows them to be used not only in perovskite–silicon tandems[11,32] but also in monolithic tandems with temperature-sensitive chalcogenide bottom cells such as CZTSSe[36] and CIGSSe.[37]

A major challenge for the future of perovskite photovoltaic devices is their stability[41] with respect to high temperature and air humidity. Particular instability was observed with mixed I–Br systems that are commonly used for band gap adjustment.[17,42] Some progress towards thermal stability has been made with formamidinium substitution[43] and introduction of a combination of formamidinium and cesium.[17,44] A remarkable V_{oc} of 1.47 V was achieved by coupling the high bandgap formamidinium bromide absorber with improved hole transporting materials based on fluorene–dithiophene derivatives. A growing number of studies continue to address the stability of perovskite interfaces under realistic operation conditions. Metal-migration induced degradation was addressed by introducing Al_2O_3 nanoparticles or chromium diffusion barriers.[45,46] Other reports claim improved stability to ambient conditions *via* a variation of the rest of the device layers.[47] It is yet to be seen if any of the proposed solutions can produce a device robust enough for practical applications.

A general challenge for perovskite tandems is the growth of the TCE on top of a device already containing a perovskite layer. Thermal and plasma damage caused by standard sputtering processes needs to be addressed. In the first reported monolithic perovskite tandem devices of type A (kesterite bottom cell), thin aluminum layers with an optical transmission of only 50% were used. The non-optimized band gap further limited the conversion efficiency to 4.7% which nevertheless was a record for any kind of chalcogenide monolithic tandem at that time.[36] This performance was soon improved to 10.9% with lower band gap CIGS bottom cells (Fig. 3) and *in situ* band-gap engineering of the perovskite top layer.[37] Thin calcium-based electrodes with an optical transmission above 85% were used in this case.

Various approaches have been employed to fabricate type A tandem devices on crystalline silicon bottom cells. Silicon p–n junctions are more resilient to thermal damage than substrate chalcogenides which expands the processing windows for layers such as TiO_2. A monolithic Si tandem device employing dense and mesoporous TiO_2 layers with a Ag-nanowire TCE on top of the spiro-OMeTAD layer covering the perovskite reached a conversion efficiency of 13.7%.[32] Protection of the underlying organic layers *via* an evaporated MoO_3 layer enabled ITO TCE to be sputtered on top of the device yielding an efficiency of 19.9% (18.1% stabilized) where the hysteresis effect was suppressed and the stability enhanced with the use of SnO_2 electron selective contact.[48] A similar approach employing MoO_3 followed by hydrogenated In_2O_3:H and ITO (Fig. 4)[33] demonstrated a monolithic perovskite tandem device with 21.2% efficiency.

Type B devices were fundamental for this rapid progress as they were used for optimizing the processing compatibility of the TCE on perovskite. Protecting the perovskite layer with non-sputtered oxide coatings has been used extensively for demonstrating semi-transparent cells with double TCEs for use in bifacial and tandem devices of type B. An evaporated MoO_3 layer in combination with an amorphous In_2O_3:H layer yielded 20.5% efficient four-terminal devices on top of a low-band gap CIGS absorber.[49] The use of lower temperature sputtering and less intense ion bombardment in comparison with standard ZnO:Al was key for achieving this performance.[49] Other approaches to protect the sensitive perovskite device structure from sputter damage include ink-based coatings such as ITO nanoparticle buffer layers before sputtered ITO. This has yielded a 25% efficient 4-terminal device on silicon. Silver nanowires were used for one of the first demonstrations of a 4-terminal perovskite tandem device that

Table 1 Survey of various high efficiency tandem perovskite devices

	Bottom cell	Tandem cell	Eff		
No	Active material	Type	(%)	Year	Ref.
1	Silicon	A/2-T monolithic	13.7	2015	32
2	Silicon	A/2-T monolithic	21.2	2016	33
3	Perovskite	A/2-T monolithic	7.0	2016	34
4	Polymer	A/2-T monolithic	16.0	2016	35
5	Silicon	B/2-T mech. stack	17.9	2014	11
6	Silicon	B/4-T mech. stack[a]	25.2	2016	17
7	Mono-crys. silicon heterojunction	B/4-T spectral split	28.0	2014	18
8	CZTS	A/2-terminal monolithic	4.6	2014	36
9	CIGS	A/2-terminal monolithic	10.9	2015	37
10	CIGS	B/2-T mech. stack	18.6	2014	11
11	CIGS	B/4-T mech. stack	20.5	2015	38

[a] Cells were measured separately, not in tandem stack.

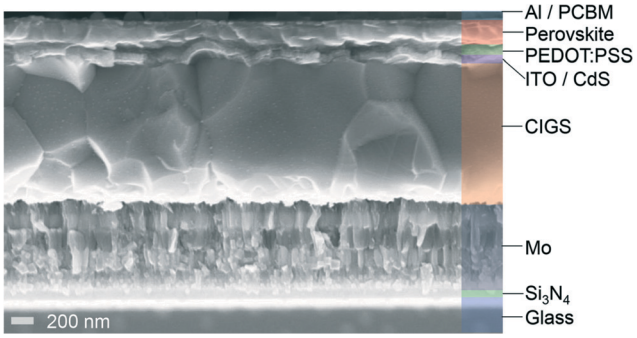

Fig. 3 SEM image of the perovskite–CIGS tandem solar cell structure, Al/PCBM/perovskite/PEDOT:PSS/ITO/CdS/CIGS/Mo/Si_3N_4/glass. Reproduced with permission.[34]

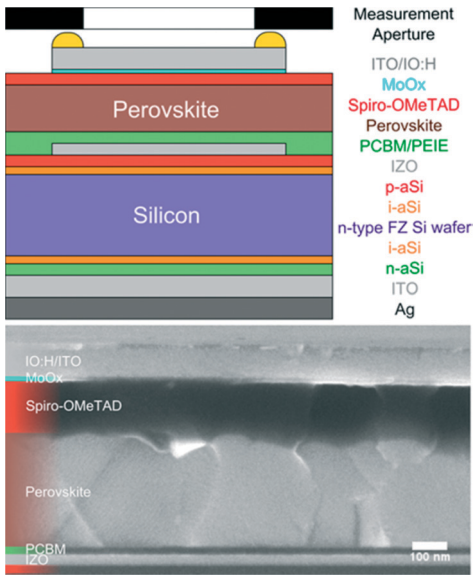

Fig. 4 Schematic drawing of the planar monolithic perovskite/silicon heterojunction tandem cell layer stack and a SEM cross-sectional view of the perovskite top cell. Reproduced with permission.[41]

yielded efficiencies of 17% with Si and 18.6% with CIGS bottom devices.[11]

Recent developments with new charge recombination layers (CRL) and soft processing conditions have taken monolithic perovskite tandem solar cells one step further with demonstrations of organic–perovskite and even pure perovskite–perovskite tandems. Graded CRL comprising C-60 derivative/Ag/MoO_3 allowed depositing a polymer device on top of a perovskite solar cell resulting in a 16% efficient tandem with low hysteresis.[35] Another CRL combination based on spiro-OMeTAD/PEDOT:PSS/PEI/PCBM:PEI[34] allowed for the first time the fabrication of monolithic perovskite–perovskite tandems. Dry layer transfer used for the PEDOT layer as well as careful selection of all processing steps helped to minimize the degradation of the full device structure. A remarkable additive V_{oc} of 1.89 V was achieved with a pair of pure iodide (low band gap) cells. The efficiency of 7% is projected to increase significantly with adequate band-gap optimization of the top cell and mitigation of the higher hysteresis effect in the full stack compared to individual devices.[34]

E. Conclusion

The unique combination of high efficiency, tunable band gap and soft processing temperature of perovskite solar cells has made them a popular partner in tandem device structures. In just a couple of years, significant progress has been achieved with both monolithic and stacked device configurations, the latter already reaching over 25% efficiency. A key factor for this success has been the development of non-destructive TCE and CRL formation techniques in order to preserve the fragile perovskite device structure. While first steps to address the long-term device stability have been taken, this remains a critical issue for the large-scale application of perovskite solar cells in general and will be decisive for their future.

References

1 D. M. Chapin, C. S. Fuller and G. L. Pearson, *J. Appl. Phys*, 1954, **25**, 676–677.
2 C. Breyer and A. Gerlach, *Progr. Photovolt.: Res. Appl.*, 2013, **21**, 121–136.
3 M. A. Green, K. Emery, Y. Hishikawa, W. Warta and E. D. Dunlop, *Progr. Photovolt.: Res. Appl.*, 2015, **23**, 1–9.
4 W. Shockley and H. J. Queisser, *J. Appl. Phys*, 1961, **32**, 510–519.
5 J. Yang, A. Banerjee and S. Guha, *Appl. Phys. Lett*, 1997, **70**, 2975–2977.
6 Accessed at http://www.ise.fraunhofer.de/en/press-and-media/press-releases/pressreleases-2014/new-world-record-for-solar-cell-efficiencyat-46-percent on 7 December 2014, 2014.
7 A. Luque and S. Hegedus, *Handbook of photovoltaic science and engineering*, John Wiley & Sons, 2011.
8 X. Wang, L. Zhi and K. Mallen, *Nano Lett.*, 2008, **8**, 323–327.
9 Z. Wu, *et al.*, *Science*, 2004, **305**, 1273–1276.
10 A. Du Pasquier, H. E. Unalan, A. Kanwal, S. Miller and M. Chhowalla, *Appl. Phys. Lett*, 2005, **87**, 203511.
11 C. D. Bailie, *et al.*, *Energy Environ. Sci.*, 2015, **8**, 956–963.
12 T. Minami, *Semicond. Sci. Technol.*, 2005, **20**, S35.
13 C. D. Bailie and M. D. McGehee, *MRS Bull.*, 2015, **40**, 681–686.
14 C.-H. Tai, C.-H. Lin, C.-M. Wang and C.-C. Lin, *Int. J. Photoenergy*, 2011, **2011**, 813093.
15 L. Wang, *et al.*, *Proceedings of the 29th EUPVSEC*, 2014, pp. 2043–2045.
16 S. Sista, Z. Hong, M. H. Park, Z. Xu and Y. Yang, *Adv. Mater.*, 2009, **22**, E77–E80.
17 D. P. McMeekin, *et al.*, *Science*, 2016, **351**, 151–155.
18 H. Uzu, M. Ichikawa, M. Hino, K. Nakano, T. Meguro, J. L. Hernandez, H.-S. Kim, N.-G. Park and K. Yamamoto, *Appl. Phys. Lett*, 2015, **106**, 013506.
19 A. De Vos, *J. Phys. D: Appl. Phys*, 1980, **13**, 839.

20 U. Rau and J. H. Werner, *Appl. Phys. Lett*, 2004, **84**, 3735.
21 This value is slightly different than the one in ref. 19 since it uses 6000 K black body spectrum instead of 1 sun AM1.5G.
22 W. N. Shafarman, R. Klenk and B. E. McCandless, *J. Appl. Phys*, 1996, **79**, 7324–7328.
23 O. Gunawan, D. B. Mitzi and T. Gokmen, *Copper Zinc Tin Sulfide-Based Thin Film Solar Cells*, John Wiley & Sons, 2015, ch. 17.
24 M. Symko-Davies and R. Noufi, in *Proceedings of 20th European Photovoltaic Solar Energy Conference, 2005*, Munich, Germany, 2005, p. 2001.
25 P. Liska, K. R. Thampi, M. Grätzel, D. Bremaud, D. Rudmann, H. M. Upadhyaya and A. N. Tiwari, *Appl. Phys. Lett*, 2006, **88**, 203103.
26 S. Nishiwaki, S. Siebentritt and P. Walk, *Progr. Photovolt.: Res. Appl.*, 2003, **11**, 243–248.
27 R. Kaigawa, K. Funahashi, R. Fujie, T. Wada, S. Merdes, R. Caballero and R. Klenk, *Sol. Energy Mater. Sol. Cells*, 2010, **94**, 1880–1883.
28 M. Reinhard, P. Sonntag, R. Eckstein, L. Barkert, A. Bauer, B. Dimmler, U. Lemmer and A. Colsmann, *Appl. Phys. Lett*, 2013, **103**, 143904.
29 J. You, *et al.*, *Nat. Commun.*, 2013, **4**, 1446.
30 C. C. Chen, W. H. Chang, K. Yoshimura, K. Ohya, J. You, J. Gao, Z. Hong and Y. Yang, *Adv. Mater.*, 2014, **26**, 5670–5677.
31 H. Zhou, Y. Zhang, C. K. Mai, S. D. Collins, G. C. Bazan, T. Q. Nguyen and A. J. Heeger, *Adv. Mater.*, 2015, **27**, 1767–1773.
32 J. P. Mailoa, C. D. Bailie, E. C. Johlin, E. T. Hoke, A. J. Akey, W. H. Nguyen, M. D. McGehee and T. Buonassisi, *Appl. Phys. Lett*, 2015, **106**, 121105.
33 J. Werner, C.-H. Weng, A. Walter, L. Fesquet, J. P. Seif, S. De Wolf, B. Niesen and C. Ballif, *J. Phys. Chem. Lett.*, 2016, **7**, 161–166.
34 F. Jiang, T. Liu, B. Luo, J. Tong, F. Qin, S. Xiong, Z. Li and Y. Zhou, *J. Mater. Chem. A*, 2016, **4**, 1208–1213.
35 Y. Liu, L. A. Renna, M. Bag, Z. A. Page, P. Kim, J. Choi, T. Emrick, D. Venkataraman and T. P. Russell, *ACS Appl. Mater. Interfaces*, 2016, **8**, 7070–7076.
36 T. Todorov, T. Gershon, O. Gunawan, C. Sturdevant and S. Guha, *Appl. Phys. Lett*, 2014, **105**, 173902.
37 T. Todorov, T. Gershon, O. Gunawan, Y. S. Lee, C. Sturdevant, L. Y. Chang and S. Guha, *Adv. Energy Mater.*, 2015, **5**, 1500799.
38 P. Reinhard, *et al.*, *PVSEC Conference*, 2015.
39 M. Liu, M. B. Johnston and H. J. Snaith, *Nature*, 2013, **501**, 395–398.
40 N. J. Jeon, J. H. Noh, W. S. Yang, Y. C. Kim, S. Ryu, J. Seo and S. I. Seok, *Nature*, 2015, **517**, 476–480.
41 A. Guerrero, J. You, C. Aranda, Y. S. Kang, G. Garcia-Belmonte, H. Zhou, J. Bisquert and Y. Yang, *ACS Nano*, 2016, **10**, 218–224.
42 E. T. Hoke, D. J. Slotcavage, E. R. Dohner, A. R. Bowring, H. I. Karunadasa and M. D. McGehee, *Chem. Sci.*, 2015, **6**, 613–617.
43 G. E. Eperon, S. D. Stranks, C. Menelaou, M. B. Johnston, L. M. Herz and H. J. Snaith, *Energy Environ. Sci.*, 2014, **7**, 982–988.
44 R. E. Beal, D. J. Slotcavage, T. Leijtens, A. R. Bowring, R. A. Belisle, W. H. Nguyen, G. F. Burkhard, E. T. Hoke and M. D. McGehee, *J. Phys. Chem. Lett.*, 2016, **7**, 746–751.
45 K. Domanski, J.-P. Correa-Baena, N. Mine, M. K. Nazeeruddin, A. Abate, M. Saliba, W. Tress, A. Hagfeldt and M. Grätzel, *ACS Nano*, 2016, **10**, 6306–6314.
46 S. Guarnera, A. Abate, W. Zhang, J. M. Foster, G. Richardson, A. Petrozza and H. J. Snaith, *J. Phys. Chem. Lett.*, 2015, **6**, 432–437.
47 A. Mei, *et al.*, *Science*, 2014, **345**, 295–298.
48 S. Albrecht, *et al.*, *Energy Environ. Sci.*, 2016, **9**, 81–88.
49 F. Fu, T. Feurer, T. Jager, E. Avancini, B. Bissig, S. Yoon, S. Buecheler and A. N. Tiwari, *Nat. Commun.*, 2015, **6**, 8932.

